Decoding Upper Limb Movement Attempt From EEG Measurements of the Contralesional Motor Cortex in Chronic Stroke Patients

Javier M. Antelis*, Luis Montesano, Ander Ramos-Murguialday, Niels Birbaumer, and Javier Minguez

***Abstract*—*Goal:* Stroke survivors usually require motor rehabilitation therapy as, due to the lesion, they completely or partially loss mobility in the limbs. Brain–computer interface technology offers the possibility of decoding the attempt to move paretic limbs in real time to improve existing motor rehabilitation. However, a major difficulty for the practical application of the BCI to stroke survivors is that the brain rhythms that encode the motor states might be diminished due to the lesion. This study investigates the continuous decoding of natural attempt to move the paralyzed upper limb in stroke survivors from electroencephalographic signals of the unaffected contralesional motor cortex. *Results:* Experiments were carried out with the aid of six severely affected chronic stroke patients performing/attempting self-selected reaching movements of the unaffected/affected upper limb. The electroencephalographic (EEG) analysis showed significant cortical activation on the uninjured motor cortex when moving the contralateral unaffected arm and in the attempt to move the ipsilateral affected arm. Using this activity, significant continuous decoding of movement was obtained in six out of six participants in movements of the unaffected limb, and in four out of six participants in the attempt to move the affected limb. *Conclusion:* This study showed that it is possible to construct a decoder of the attempt to move the paretic arm for chronic stroke patients using the EEG activity of the healthy contralesional motor cortex. *Significance:* This decoding model could provide to stroke survivors with a natural, easy, and intuitive way to achieve control of BCIs or robot-assisted rehabilitation devices.**

***Index Terms*—Brain–computer interface (BCI), movement decoding, stroke, uninjured motor cortex.**

Manuscript received April 27, 2015, September 20, 2015, and February 13, 2016; accepted March 8, 2016. Date of publication March 24, 2016; date of current version December 20, 2016. This work was supported in part by the Mexican National Council for Science and Technology, Spanish Ministry of Science Projects HYPER-CSD2009-00067, DPI2009-14732-C02-01, DPI2011-25892, the Deutsche Forschungsgemeinschaft, the German Ministry of Education and Research, Bernstein Centers 01GQ0761, BMBF 58416SV3783, the EU HUMOUR-ICT-2008-231724, the Baden-Wuttember Stiftung C. and the Baden Wuerttemberg Stiftung (ROB-1), Daegu Gyeongbuk Institute of Science and Technology, and the Ministry of Education, Science and Technology of Republic of Korea and the CORBYS EU project No. 270219. *Asteric indicates corresponding author.*

*J. M. Antelis is with the Tecnológico de Monterrey, Campus Guadalajara, Zapopan 45201, México (e-mail: mauricio.antelis@gmail.com).

L. Montesano is with the Instituto de Investigación en Ingeniería de Aragón (I3A).

A. Ramos-Murguialday is with the Institute of Medical Psychology and Behavioral Neurobiology, Eberhard-Karls-University, and also with TECNALIA, Health Technologies.

N. Birbaumer is with the Institute of Medical Psychology and Behavioral Neurobiology, Eberhard-Karls-University, and also with the Istituto di Ricovero e Cura a Carattere Scientifico.

J. Minguez is with the Instituto de Investigación en Ingeniería de Aragón, and also with, Bit&Brain Technologies SL.

This paper contains supplemental material available online at http://ieeexplore.ieee.org (File size: 1 MB).

Digital Object Identifier 10.1109/TBME.2016.2541084

I. Introduction

STROKE is the leading cause of paralysis in adults and the elderly [1], therefore there is an increasing interest in interventions to improve the rehabilitation of stroke survivors [2], [3]. Robot-assisted rehabilitation therapies have emerged providing reliable and safe ways for rehabilitation of the affected limbs. Numerous benefits have been reported, including the enhancement of muscle strength, improvement of motor coordination and dexterity, reduction of the therapist's assistance time, and promotion of neural circuit strength to recover lost mobility [4], [5].

Many of the robot-assisted motor rehabilitation therapies rely on the patient's attempt to move, based on residual movements. This information is usually obtained from force and kinematic sensors [6], [7], electromyographic (EMG) activity, or from the combination of both [8]–[11]. For patients without any residual movement in the affected limbs, EMG (if present) or electroencephalographic (EEG) activity or near-infrared spectroscopy, alone or in combination with EMG, might be the only noninvasive remaining signals that could be used to trigger the robotic device in a natural way (closing the loop between the intention of movement and the mobilization of the paralyzed limb [12], [13]). Promotion of motor relearning has been suggested to occur when the patient's motor state (the attempt to move the paralyzed limbs) is directly extracted from the central nervous system rather than from the peripheral one [14], [15]. However, the practical applicability of these principles to stroke patients might be hindered by the damage suffered in the brain and its effects on the motor rhythms that encode movement. This study reports the possibility of continuous decoding the natural movement attempt of the paretic upper limb from the EEG activity recorded from the healthy motor cortex of the patient.

The decoding of motor information from EEG activity has been demonstrated in healthy individuals [17]–[20] and in patients with spinal cord injuries [21], [22] or amyotrophic lateral sclerosis [23]. In stroke survivors, recent works have studied the effects on the rehabilitation status and on the brain activation using EEG-based brain–computer interfaces (BCIs)

TABLE I
DEMOGRAPHIC AND CLINICAL INFORMATION OF THE SIX STROKE PATIENTS USING A MODIFIED UPPER LIMB FUGL-MEYER ASSESSMENT [16] (MAXIMAL SCORE IS 114 POINTS; VALUES 0-2, 0 = NO ACTIVITY, 1 = PARTIAL ACTIVITY; 2 = PERFECT ACTIVITY)

Patient	Age	Gender	Dominant Hand	Years since stroke	Hemisphere of stroke	Lesion location	Lesion information	Fugl-Meyer score (arm)
P1	50	M	R	1.4	Left	Cortical/Subcor.	Corona radiata, capsula externa, claustrum	$\frac{0}{24}+\frac{2}{32}$
P2	56	M	R	2.8	Right	Cortical/Subcor.	Frontal, parietal and temporal lobe. Middle and inferior frontal gyrus; pre and postcentral gyrus; supramarginal gyrus; angular gyrus. Trunk of corpus callosum	$\frac{3}{24}+\frac{6}{32}$
P3	52	M	R	18	Left	Cortical/Subcor.	Corona radiata, CI, genu, thalamus, external capsule, putamen, claustrum, insula and adjacent white matter	$\frac{11}{24}+\frac{2}{32}$
P4	60	M	R	1.2	Right	Cortical/Subcor.	Parietal and occipital lobe and the adjacent white matter, multiple necrotic vesicles in the parietal lobe underneath the post-central and precentral gyrus	$\frac{3}{24}+\frac{11}{32}$
P5	53	F	R	1.7	Left	Subcortical	Frontal and parietal lobe and adjacent white matter with multiple necrotic. Middle and inferior frontal gyrus; pre and postcentral gyrus; middle temporal gyrus	$\frac{0}{24}+\frac{2}{32}$
P6	40	M	R	6.8	Right	Subcortical	CI, genu, external capsule, claustrum, putamen, head of caudate nucleus, thalamus	$\frac{3}{24}+\frac{12}{32}$

[24]–[26]. However, as the lesion usually affects motor neural networks that connect intention with action, it might alter the EEG motor-related patterns in the lesional and perilesional brain areas associated with paretic limbs, therefore reducing performance in BCI-based rehabilitation scenarios [27]. Functional magnetic resonance imaging and invasive studies have shown the existence of ipsilateral cortical activity associated with limb movements [28]–[31], which is assumed to be due to subcortical and intercallosal and interhemispheric connections [32], [33]. This suggests the possibility of decoding motor information associated with paralized limbs using brain signals from other areas that are different from the damaged hemisphere, in particular the contralesional side. Indeed, previous works have shown that the power spectra of EEG signals from the healthy motor cortex of stroke survivors could be utilized to control a BCI based on motor imagery [34].

This study shows that it is possible to construct a continuous decoder of the attempt to move the paretic arm for severely-affected chronic stroke patients using the EEG activity of the healthy contralesional motor cortex. The results of the paper extend those presented in [35]. First, the decoding method exploits the temporal structure of the intervention to obtain significantly better results. Second, this study describes a deeper analysis of the decoding accuracy using brain signals from the injured ipsilesional, uninjured contralesional, and both motor cortex, over an extended set of six participants. A continuous decoding of movement information is a more natural way to integrate such information in rehabilitation scenarios, as the technology can continuously estimate the patient's attempt to move, and drive the rehabilitation robot online [36].

II. METHODS

A. Participants

The experiments were approved by the ethics committee of the Medical Faculty, University of Tübingen, and all participants provided informed consent. Twelve patients (age range 40–60 years) were enrolled in this study. However, data of six of them were discharged as they fulfilled with one of the exclusion criteria (see section *Dataset's exclusion criteria*). Demographic and clinical information of the six remaining participants is shown in Table I. All participants suffered a unilateral subcortical or mixed cortical stroke (three in the left and three in the right hemisphere) and were in the chronic stage (> 1.2 years since stroke). The participants did not exhibit attention deficits, aphasia, or any other cognitive impairment that could restrict the understanding or execution of the experiment. The participants were not able to use the paretic upper limb for any daily living activity and presented no residual finger extension.

B. Data Acquisition

EEG data were recorded using a 64-channel BrainAmp amplifier and an actiCAP system for active electrodes (from Brain Products GmbH, Munich, Germany). The 64 electrodes were uniformly distributed on the scalp, following the $10/10$ international system with the ground at AFz and referenced to the nasion. EMG data were recorded from the eight muscles of each arm: 1) extensor carpi ulnaris, 2) extensor digitorum, 3) flexor carpi radialis, plamaris longus, flexor carpi ulnaris (flexion), 4) external head of the biceps (flexion), 5) external head of the triceps, 6) frontal side of the deltoid, 7) lateral side of the deltoid, and 8) posterior side of the deltoid over the teres minor and infraspinatus muscles. These EMG signals were recorded using bipolar Ag/AgCl electrodes (from Myotronics-Noromed, USA) and two 16-channel BrainAmp amplifiers. The EEG and EMG electrode impedance was maintained under 5 and 20 kΩ, respectively. EEG and EMG signals were recorded at a sampling rate of 2500 Hz with no filtering (using the BrainAmp amplifier and BrainVision Recorder software from Brain Products GmbH, Germany).

C. Experimental Procedure

The participants were seated in a chair, in front of a computer screen, with both forearms resting comfortably on their lap. The execution of the experiment was controlled by visual and auditory cues, which were presented simultaneously. The experiment consisted of trials in two movement conditions: 1) execution of reaching movements toward self-selected targets with the unaffected limb (condition 1), and 2) attempting to perform the same reaching movements but with the paretic limb (condition 2). Fig. 1 displays snapshots of the two experimental conditions for a participant with the lesion in the left hemisphere and illustrates the temporal sequence of a trial in the experiment. Each trial started with a first cue indicating the users to relax the body and to adopt the initial position, which lasted 3 s. A second cue indicated the users to perform or to attempt to perform, during 3 s, the hand reaching movement toward a self-selected (one out of the three) target presented on the screen. Patients were asked to consider the reaching as successful when the visual trajectory to the target presented on the screen was intersected with the hand if they performed movements with the unaffected limb, or when the three targets disappeared from the screen if they were attempting to move the affected limb. A third cue indicated the users that they could rest and relax while adopting the initial position, which also lasted 3 s. During the first two phases of each trial (between the first and third cues), participants were asked to avoid blinking or compensatory movements. A visual presentation program (developed in e-prime) presented the visual and auditory cues that controlled timing sequence of the trials and sent synchronization signals to the EEG and EMG recording system. The experiment was divided into four blocks (two of each movement condition) of 40 trials each, resulting in a total of 160 trials (80 for each condition). Patients could rest between blocks and whenever needed to avoid fatigue. The execution of this experimental task was constantly monitored by the experimenter, who had to report situations and issues about the participants, the signals, and the experiment.

D. Dataset's Exclusion Criteria

After the execution of the experimental procedure, the full dataset of any of the participant was discharged and not used in the study if it fulfilled one of the exclusion criteria: 1) the experimenter reported that the participants recursively intended to compensate the attempt to move the affected paretic arm (i.e., experimental condition 2) with the torso and other body parts, 2) the subsequent visual inspection of the EEG traces revealed that the recorded signals were contaminated with artifacts.

E. EEG and EMG Data Preprocessing

For each participant, EEG and EMG data were segmented in trials of 9 s using the second cue as reference, thus each trial lasted from -3 to 6 s. Subsequently, each trial was again trimmed to the interval from -3 to 3 s relative to the EMG-based movement initiation. Therefore, each trial was composed by the rest phase $[-3, 0)s$ followed by the motion phase $[0, 3)s$. This EMG-based movement onset was computed independently for each subject and experimental condition following this procedure: 1) the EMG channel across all trials with the most consistent activity (i.e., low amplitude in the rest phase and sustained high amplitude in the motion phase) from all eight muscles of the used limb according to the experimental condition was selected by visual inspection; 2) this EMG signal was high-pass filtered with a cutoff frequency of 10 Hz and its envelope was computed using the Hilbert-transform; 3) the time latency of the first data point in the EMG envelope whose value is 10% of the envelope's maximum value was detected and defined as the movement onset provided that this time instant is greater than the time of the second cue (initiation of the reaching movement phase) and less than the time of the third cue (end of the reaching movement phase), i.e., the EMG-based movements onset is at some time within the motion phase. This onset was validated through visual inspection of the time-resolved EMG activity along with the latency of the detected onset; 4) in case that no onset was detected for a given trial, the EMG-based movement onset was set by visual inspection using the EMG of all muscles. Finally, all EEG trials were bandpass-filtered from 0.5 to 60 Hz using a zero-phase shift filter, re-sampled to 160 Hz, and Laplacian-filtered to remove the effects of volume conduction [37].

F. EEG Data Analysis

To study the task-related power spectra changes of the EEG activity, significant maps of event-related power desynchronization/synchronization or ERDS(t, f) maps were computed for each experimental condition. First, for each trial and electrode, the time-frequency representation TFR(t, f) was computed using complex Morlet wavelets [38] in the frequency range between 2 and 40 Hz at the resolution of 1 Hz. The family of wavelets was $w(t, f) = Ae^{-t^2/2\sigma_t^2}e^{2\pi ift}$ with $A = (\sigma_t \pi^{1/2})^{-1/2}$ and $\sigma_t = 1/2\pi\sigma_f$, which is characterized by the constant tradeoff ratio f/σ_f that is typically fixed to 7 for the analysis of EEG signals [39] (higher values of f/σ_f increase the frequency resolution while lower values increase the temporal resolution [38]). Subsequently, the averaged time-frequency representation of each electrode $P(t, f)$ was computed across all trials, and the map of event-related power desynchronization/syncronization, defined as the percentage of power increase/decrease relative to the power in the rest phase $[-3, 0)s$ was computed as ERDS$(t, f) = 100 * (P(t, f) - P_{\text{rest}}(f))/P_{\text{rest}}(f)$, where $P(t, f)$ is the power spectra at time t and frequency f and $P_{\text{rest}}(f)$ is the average power spectra at the rest phase ($[-3, 0)s$) for frequency f. Finally, significant power increases or decreases in the ERDS(t, f) map were computed with a bootstrap analysis at the significance level of $\alpha = 0.05$ [40] using as baseline the time interval of the rest phase $[-3, 0)s$.

Dynamical imaging of coherent sources [41] was applied to estimate the neural sources of the oscillatory EEG activity in the motor-related α and β frequency bands. This technique estimates the power of the neural sources by contrasting the differences between two conditions, in our case rest phase $[-3, 0)$s and the motion phase $[0, 3)$s, based on a common spatial filter for each neural source. The spatial filter is derived from the

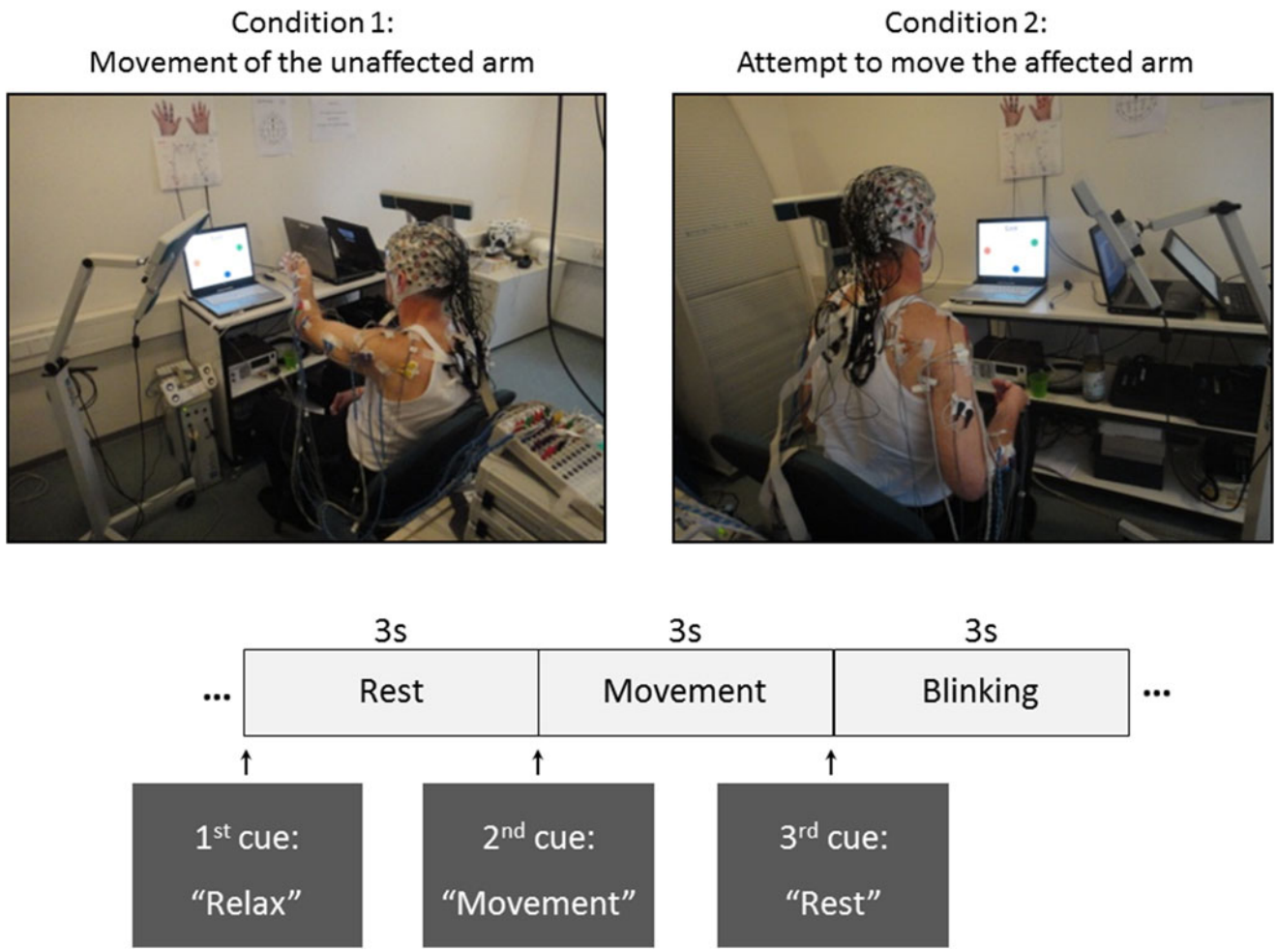

Fig. 1. Snapshots of a participant with the lesion in the left hemisphere while performing the experimental task: upper left panel shows the execution of reaching movements with the unaffected left limb toward one out of three self-selected targets presented on the computer screen, while upper right panel shows the attempt to perform the same reaching movements toward a self-selected target with the paretic right limb. Lower panel shows the timing sequence of a trial of the experiment.

cross-spectral density of the EEG activity and the lead field provided by the brain template of the Montreal Neurological Institute [42].

Both types of analyses, ERDS and source localization, were carried out independently for each experimental condition, first, for all participants with the lesion in the same hemisphere, and second, for each participant individually.

G. EEG Feature Extraction and Selection

The power spectra of the ongoing EEG activity was used as features to continuously decode the movement of the unaffected and affected arm. For each trial, the set of features O_k at time k ($k \in [-3, 3)$) were computed using the EEG in the time window $[k-\delta, k]$ (where $\delta = 0.75$ s is the length of window). Following previous studies [43], [44], the power spectra was estimated using a 16th-order autoregressive model and the Burg's method to estimate the coefficients and noise variance [45]. As we aimed to evaluate the continuous decoding of movement using brain signals from the motor cortex in the ipsilesional, contralesional, and both hemispheres, the power spectra-based features were selected solely from channels located above the injured motor cortex and the uninjured motor cortex, and from frequencies within the motor-related frequency bands (α $(8-12\,\mathrm{Hz})$, μ $(12-15\,\mathrm{Hz})$, and β $(15-30\,\mathrm{Hz})$). The selection of channels and frequencies was based on 1) the highest r-squared values between the rest phase and the motion phase (computed as the square of the Pearson's correlation between the feature and the labels, [46]), and 2) significant power desynchronization in the time interval of the motion phase (i.e., $[0, 3)$s).

H. Continuous Decoding of Movement

The continuous decoding of movement aims to estimate the unknown movement state $S_k \in \{\mathrm{rest}, \mathrm{motion}\}$, based on the temporal sequence of observed features $O_{1:k} = (O_1, O_2, \ldots, O_k)$, up to time k where $k \in [-3, 3)$. This has been usually done by training classifiers such as linear discriminant analyses or support vector machines (SVM). Sliding a window is used to deal with the continuous EEG signal [36], [47], [48]. For motor imagery, hidden Markov models (HMM) have been used to incorporate the temporal structure in asynchronous detectors

[49]–[51]. The HMM model takes advantage of the prior knowledge on the temporal structure of the sequence (e.g., the rehabilitation protocol) that induces a transition model $p(S_k \mid S_{k-1})$ for the temporal sequence $S_{1:n} = (S_1, S_2, \ldots, S_k, \ldots, S_n)$. The transition model is a discrete probability distribution between the two possible values of the state S_k. For the likelihood model $p(O_k \mid S_k)$, it is common to use Gaussian models or a mixture of Gaussians (see [49]–[51] for BCI applications). The performance of HMM can be degraded if the observations of the different states lead to probability functions that overlap, as it occurs with the power spectra during rest and movement, especially during the transition from rest to motion. Therefore, instead of modeling the probability of the observations for the different states $p(O_k \mid S_k = i)\ \forall\ i \in \{\text{rest}, \text{motion}\}$, the conditional probability of states given the observations $p(S_k = i \mid O_k)\ \forall\ i \in \{\text{rest}, \text{motion}\}$ was computed using SVM. This computation is based on the distance of the feature vector O_k to the hyperplane separating both classes, which is transformed into the class probability using the sigmoid function

$$p(S_k = \text{motion} \mid O_k) = \frac{1}{1 + \exp(Af(O_k) + B)}$$

where $f(O_k)$ is the output of the SVM for observation O_k, and the parameters A and B are obtained through maximum likelihood [52]. The probability of the observations for the different states $p(O_k|S_k = i)\ \forall\ i \in \{\text{rest}, \text{motion}\}$ is obtained by applying the Bayes' rule with an uniform probability for the observations $p(O_k)$, and the empirical frequency of each class for $p(S_k)$.

The proposed method has a certain number of parameters that were learned from the data: 1) initial state probability vector $p(S_0 = i)\ \forall\ i \in \{\text{rest}, \text{motion}\}$2) state transition matrix π, where $\pi_{\text{ij}} = p(S_k = i|S_{k-1} = j)$, and 3) likelihood functions $p(O_k|S_k = i)\ \forall\ i \in \{\text{rest}, \text{motion}\}$, which were computed from the class probability provided by the SVM with a radial basis function kernel. The kernel hyper-parameters were set to $C = 1$ for the regularization parameter and $\sigma = 0.5$ for the RBF width [47], [53].

I. Evaluation and Metrics

The accuracy of the decoding model for each experimental condition was assessed by chronological ten-fold cross-validation. Preprocessing and feature extraction were obtained independently for each fold. For each trial in the training, features were computed from nonoverlapping sliding windows (i.e., $k \in \{-3 + \delta, -3 + 2\delta, \ldots, 3\}$). Features were z-score normalized, and labeled as rest when computed in the time interval $[-3, 0)$s, and motion when computed within the time interval $[\delta, 3)$s. These pairs of features and labels were used to estimate the model parameters. Once the model was learned, test trials were classified using features extracted every 50 ms (i.e., the step of the sliding window). The time-resolved decoding accuracy (tDA_k) was defined as the accuracy of the classification at each time in the interval $[-3 + \delta, 3)$. The decoding accuracy in rest (DA_{rest}) was computed as the mean tDA_k in the rest phase $[-3 + \delta, 0)s$. The decoding accuracy in motion (DA_{motion}) was computed as the mean tDA_k in the motion phase $[0, 3)s$. The total decoding accuracy (DA_{total}) was the mean tDA_k in both phases $[-3 + \delta, 3)s$.

The chance level of the decoding accuracy was empirically obtained by using a shuffling version of the training data, i.e., for the training of the SVM, the labels $\{\text{rest}, \text{motion}\}$ were randomly assigned to the corresponding extracted features O_k. This shuffling process was repeated ten times (per participant) to avoid chance effects due to the stochastic nature of the process.

III. Results

Data from six of the participants were excluded from the study. On the one hand, the experimenter reported that these participants recursively intended to compensate movement in the execution of experimental condition 2 (i.e., attempt to move the affected arm) with the torso and other body parts, even though they were constantly advised not to do so. On the other hand, the visual inspection of the EEG traces revealed that the data from these participants were highly noisy and contaminated with EMG activity, especially during the motion phase. Therefore, data from these six participants were discharged and not used to evaluate the continuous decoding of movement.

For the six remaining participants, the EMG-based movement onset was detected for all trials, experimental conditions and participants just after the presentation of the second cue (i.e., the one that instructed to perform or to attempt to perform the movement). The selected EMG channel varies for all participants and experimental condition. Fig. 2(a) shows the time-resolved amplitude envelope of the EMG activity averaged across all trials for participant P1. The averaged amplitude in condition 1 was 8.63 ± 6.31 and 88.89 ± 38.80 mV for rest and motion, respectively, while in condition 2 it was 12.93 ± 13.45 and 66.83 ± 42.73 mV for rest and motion, respectively. Note that in both conditions the amplitude is consistently lower in rest than in motion, and that amplitude during motion is higher in condition 1 than in condition 2. The detected movement onset averaged across all subjects was 0.54 ± 0.27 s for condition 1 and 0.66 ± 0.35 s for condition 2. Thus, the EMG-based movement onset is lower in condition 1 (i.e., movement of the unaffected arm) than in condition 2 (i.e., attempt to move the affected arm).

As illustration, Fig. 2(b) shows the raw EMG activity of one representative trial for each experimental condition of participant P1 which has the lesion in the left hemisphere. In condition 1, EMG activation is observed in signals recorded from the left unaffected arm (most of these eight EMG channels show low amplitude in the rest phase $[-3, 0)$s and high amplitude in the motion phase $[0, 3)$s), but not in signals recorded from the right affected arm. In condition 2, the EMG activation is observed solely in signals recorded from the right affected arm, however, the EMG amplitude is lower and less channels show consistent activity during the trial (i.e., low amplitude in the rest phase and high amplitude in the motion phase). For these two representative trials, the EMG-based movement onset is 0.36 and 0.66 s for condition 1 and 2, respectively.

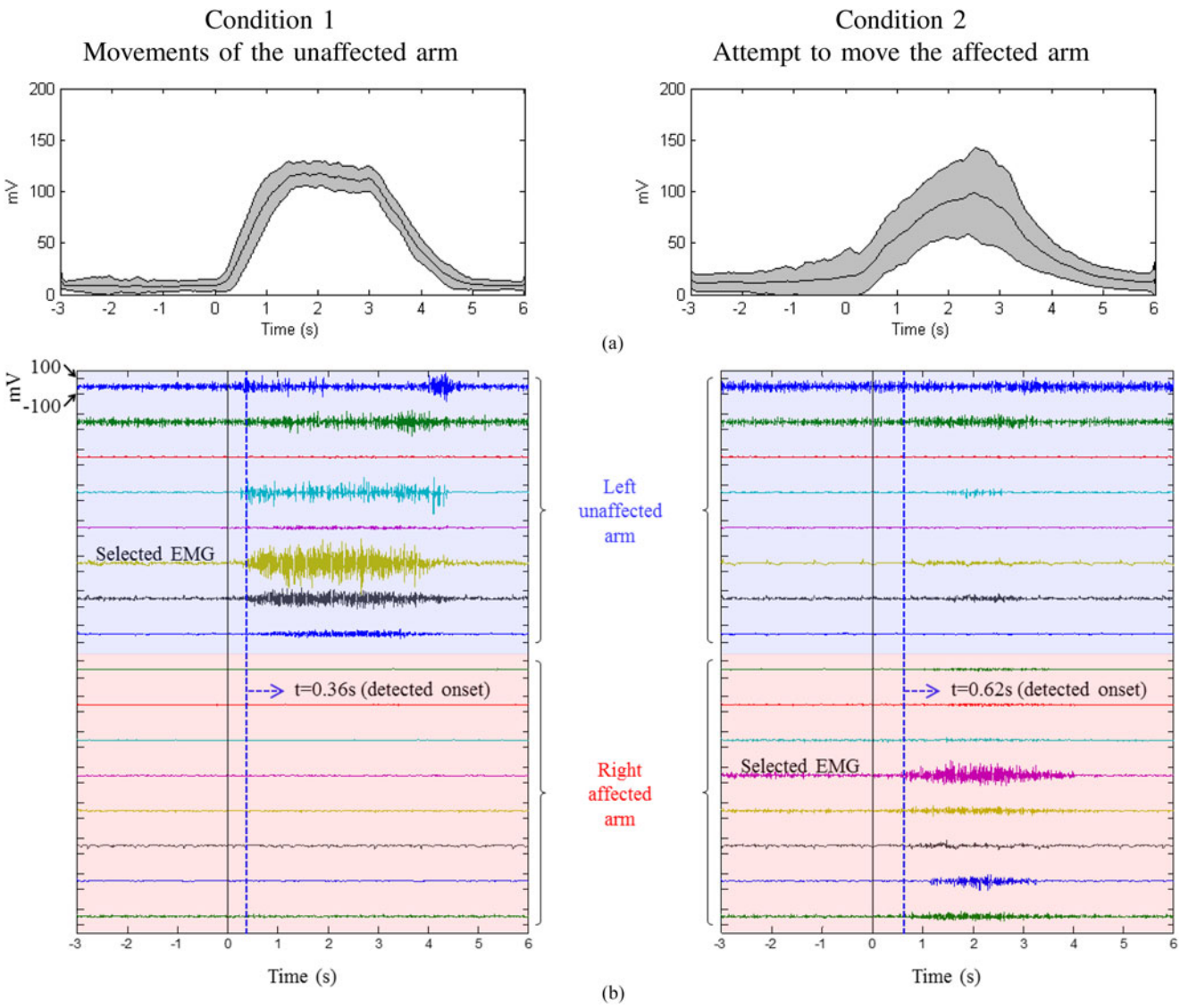

Fig. 2. (a) Time-resolved amplitude envelope of the EMG activity averaged across all trials in both experimental conditions for participant P1. (b) Raw EMG activity of participant P1 (lesion in the left hemisphere) for two representative trials (one for each experimental condition). The plots show the bipolar EMG signals recorded from the eight muscles in each arm and the selected EMG signal used to compute the EMG-based movement onset.

In the EEG analysis, the participants were divided into two groups according to the location of the lesion (three participants suffered left cortex lesion, and three suffered right cortex lesion). The results are summarized in Fig. 3.

In condition 1, significant event-related power desynchronization/synchronization activity ($p < 0.05$) was observed in sensors located above the contralateral uninjured cortex (top of panels A and D). For instance, the average of significant event-related power desynchronization/synchronization activity for the $[10, 20]$Hz frequency band was -19.19% in CP4 (sensor located in the right uninjured cortex for the group of participants with left cortex lesion), while it was -30.40% in CP3 (sensor located in the left uninjured cortex for the group of participants with right cortex lesion). No significant event-related power desynchronization/synchronization activity ($p > 0.05$) was found in the sensors located above the ipsilateral injured cortex (top of panels A and D). The maximum of the oscillatory neural activity in the $[10, 20]$Hz frequency band was estimated on the contralateral uninjured motor cortex in Brodmann Area 6 for the group of participants with left cortex lesion, and in Brodmann Area 40 for the groups of participant with right cortex lesion (bottom of panels A and D).

In condition 2, significant event-related power desynchronization/synchronization activity ($p < 0.05$) was observed in sensors located in the ipsilateral uninjured cortex (top of panels B and F). For instance, the average of significant event-related power desynchronization/synchronization activity for the $[10, 20]$Hz frequency band was -15.24% in CP4 (sensor located in the right uninjured cortex for the group of participants suffering from left cortex lesion), and -14.71% in CP3 (sensor located in the healthy left uninjured for the group of participants with right cortex lesion). No significant event-related power desynchronization/syncronization activity ($p > 0.05$) was observed in sensors above the contralateral injured cortex (top of

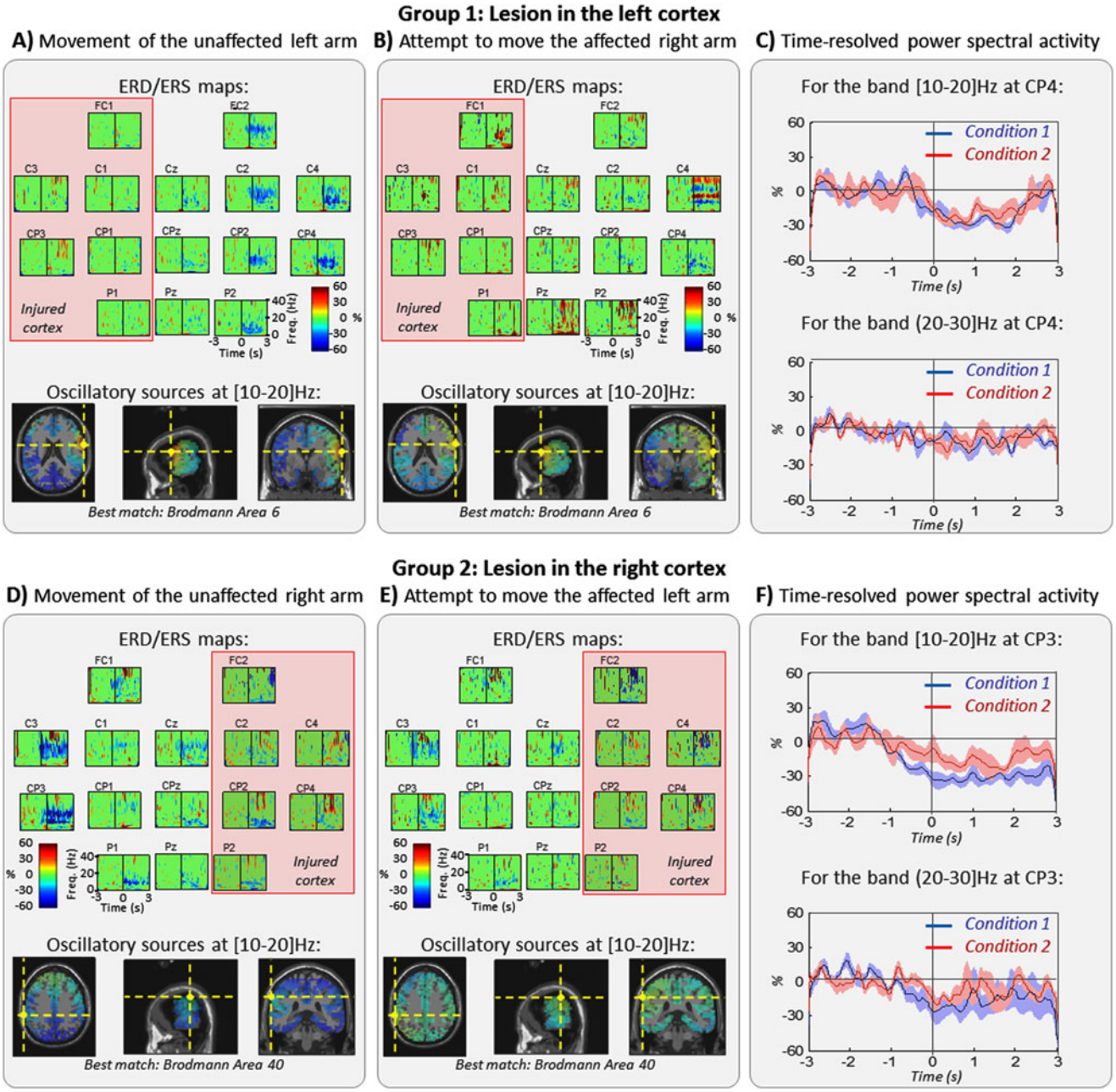

Fig. 3. Significant event-related power desynchronization/synchronization maps, oscillatory neural sources at the frequency band [10–20] Hz and time-resolved power spectral activity for the three participants with lesion in the left hemisphere (Panels A, B, and C) and for the three of participants with lesion in the right hemisphere (Panels D, E, and F). Significant desynchronization is plotted as blue (negative values), significant synchronization is plotted as red (positive values), while no significant desynchronization/synchronization is observed as green (zero values). Red boxes in the $\mathrm{ERDS}(t,f)$ maps wrap the sensors located above the injured hemisphere. Panels A and D show the $\mathrm{ERDS}(t,f)$ maps for condition 1 (movement of the unaffected arm). These maps show significant desynchronization in the uninjured (contralateral) cortex and no significant desynchronization in the injured (ipsilateral) cortex. The corresponding oscillatory sources were estimated in the uninjured cortex (bottom of panels A and D). Panels B and E show the $\mathrm{ERDS}(t,f)$ maps for condition 2 (attempt to move the affected arm). These maps show significant desynchronization in the uninjured (ipsilateral) cortex and no significant desynchronization in the injured (contralateral) cortex. The oscillatory sources were also estimated in the uninjured cortex (bottom of panels B and E). Panels C and F show the averaged time-resolved power spectral activity at the $[10–20]$ and $[20–30]$ Hz bands in CP3 and CP4 (sensors over the uninjured motor cortex), respectively.

panels B and F). The maximum of the oscillatory neural activity in the $[10, 20]$Hz frequency band was estimated on the ipsilateral uninjured motor cortex in Brodmann Area 6 for the group of participants with left cortex lesion; and in Brodmann Area 40 for the group of participants with right cortex lesion (bottom of panels B and F).

For both group of participants, the time-resolved power spectral activity shows stronger power desynchronization in condition 1 (movement of the unaffected arm) than in condition 2 (attempt to move the affected arm) for the frequency band $[10-20]$Hz (top of panels C and F), while the differences between the two conditions are less notice-

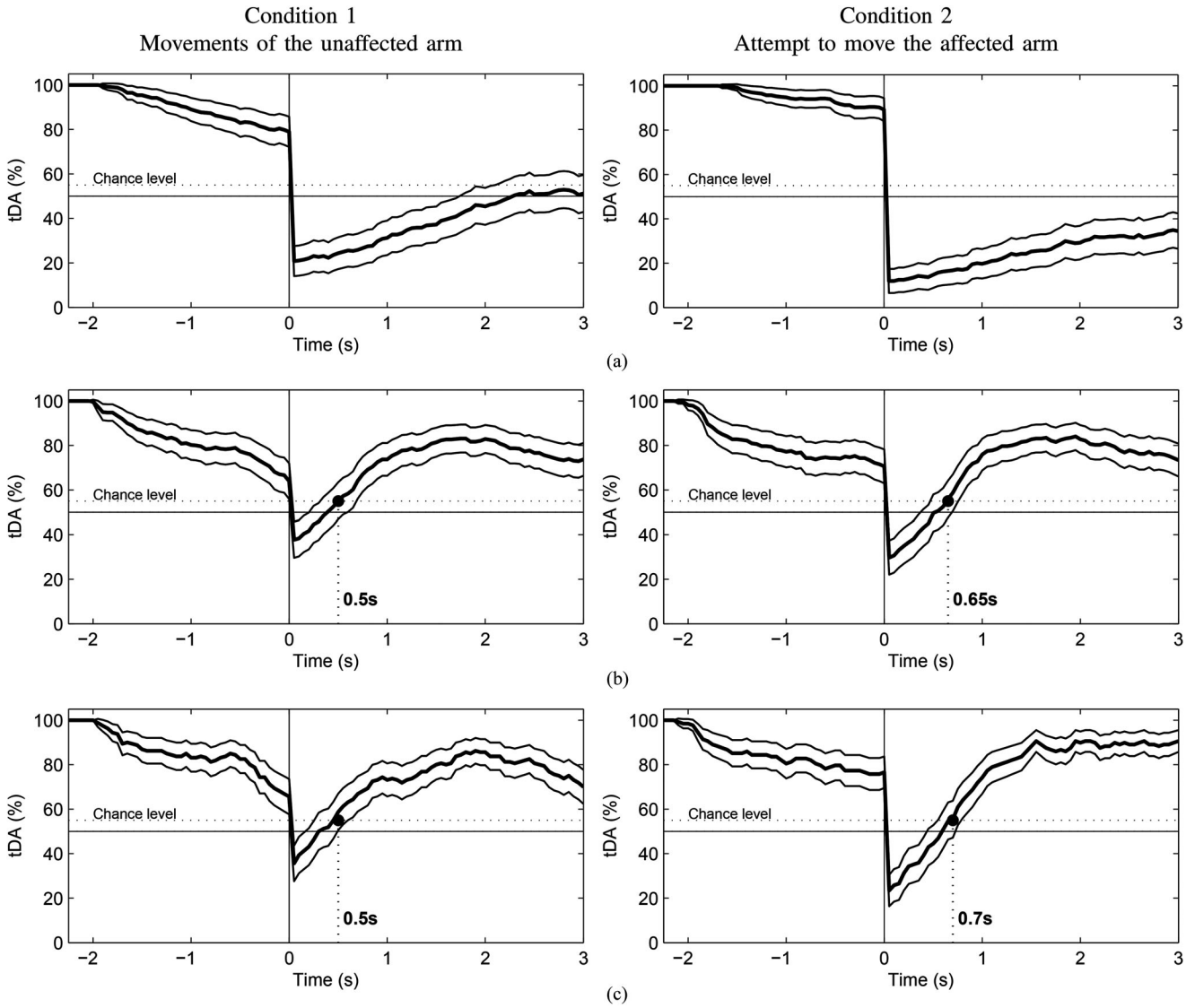

Fig. 4. Time-resolved decoding accuracy or tDA_k results averaged across all participants using channels from (a) the injured motor cortex, (b) the uninjured motor cortex, and (c) both the injured and uninjured motor cortex. tDA_k before $t = 0$ (i.e., the EMG-based movement onset) corresponds to the rest phase, while after $t = 0$ corresponds to the motion phase. The dotted line in all plots indicates the significant chance level.

able for the frequency band $[20 - 30]$Hz (bottom of panels C and F).

Regarding the feature extraction process, the r-squared analysis revealed for all participants differences between movements of the unaffected arm or the attempt to move the affected arm (motion phase $[0, 3)$s) with respect to the nonmovement period (rest phase $[-3, 0)$ s). In the two conditions, the differences were observed in the sensors located above the uninjured contralesional motor cortex, they were subject-specific and presented slight variations across the sensors and on the motor frequencies. No differences were observed in the sensors located above the injured motor cortex (see Figures S1 and S2 of the supplementary results the topographical map of r-squared values and the scalp topographies at the most discriminant frequencies for participants P1, lesion in the left hemisphere, and P4, lesion in the right hemisphere). These results are in agreement with the previous event-related power desynchronization/synchronization analyses. To evaluate the continuous decoding of movement using brain signals from the injured motor cortex, the uninjured motor cortex, and both the injured and uninjured motor cortex, sensors above the injured and uninjured motor cortex and frequencies in the motor-related bands (α, μ and β) with the highest r-squared values and with significant power desynchronization in the time window of the motion phase $[0, 3)s$ were selected as features.

Fig. 4 shows the time-resolved decoding accuracy metric tDA_k averaged across all participants for the proposed decoding model based on SVM+HMM. Note that with brain signals from the injured cortex [see Fig. 4(a)], tDA_k in both conditions is always above the significant chance level in the rest phase, but it is always below this level in the motion phase. Therefore, no significant continuous decoding of movement is possible

TABLE II

AVERAGE OF THE DECODING ACCURACY METRICS (DA_{rest}, DA_{motion}, AND DA_{total}) FOR ALL PARTICIPANTS AND THE AVERAGE ACROSS ALL OF THEM USING EEG SIGNALS FROM (A) THE INJURED MOTOR CORTEX, (B) THE UNINJURED MOTOR CORTEX, AND (C) BOTH THE INJURED AND UNINJURED MOTOR CORTEX

	Condition 1: Movements of the unaffected arm			Condition 2: Attempt to move the affected arm		
	DA_{rest}	DA_{motion}	DA_{total}	DA_{rest}	DA_{motion}	DA_{total}
P1	97 ± 04	35 ± 13	62 ± 19	93 ± 06	32 ± 12	58 ± 16
P2	93 ± 09	42 ± 14	64 ± 19	100 ± 1	07 ± 03	47 ± 13
P3	80 ± 12	56 ± 14	67 ± 13	94 ± 05	35 ± 09	61 ± 17
P4	80 ± 14	58 ± 10	68 ± 15	95 ± 05	26 ± 07	56 ± 17
P5	99 ± 01	16 ± 06	52 ± 16	94 ± 05	29 ± 11	58 ± 16
P6	95 ± 05	22 ± 10	54 ± 16	100 ± 0	11 ± 04	49 ± 16
All	91 ± 07	38 ± 11	61 ± 15	96 ± 04	24 ± 07	55 ± 15

(a)

	DA_{rest}	DA_{motion}	DA_{total}	DA_{rest}	DA_{motion}	DA_{total}
P1	84 ± 12	72 ± 11	77 ± 13	90 ± 04	71 ± 25	79 ± 09
P2	88 ± 07	67 ± 17	76 ± 12	99 ± 01	15 ± 07	51 ± 16
P3	85 ± 10	68 ± 13	75 ± 13	83 ± 10	73 ± 15	77 ± 11
P4	81 ± 10	73 ± 15	76 ± 11	79 ± 11	65 ± 16	71 ± 12
P5	79 ± 12	72 ± 13	75 ± 12	89 ± 11	47 ± 07	65 ± 18
P6	85 ± 11	75 ± 15	79 ± 11	75 ± 15	71 ± 11	73 ± 13
All	84 ± 10	71 ± 13	77 ± 11	84 ± 08	62 ± 14	72 ± 11

(b)

	DA_{rest}	DA_{motion}	DA_{total}	DA_{rest}	DA_{motion}	DA_{total}
P1	84 ± 12	71 ± 12	77 ± 13	90 ± 04	72 ± 24	80 ± 10
P2	90 ± 08	70 ± 15	79 ± 14	100 ± 0	14 ± 10	51 ± 21
P3	80 ± 13	71 ± 15	75 ± 13	77 ± 14	83 ± 18	80 ± 16
P4	87 ± 07	78 ± 15	82 ± 11	86 ± 09	67 ± 25	75 ± 13
P5	92 ± 11	70 ± 19	80 ± 19	90 ± 13	44 ± 13	64 ± 22
P6	88 ± 10	75 ± 19	81 ± 14	65 ± 20	81 ± 13	74 ± 18
All	86 ± 09	72 ± 13	78 ± 12	86 ± 07	69 ± 20	76 ± 10

(c)

with EEG signals of the ipsilesional motor cortex. However, with brain signals from the uninjured and from both the injured and uninjured motor cortex (see Fig. 4(b) and (c), respectively), tDA_k in both conditions is above the significant chance level in the whole rest phase and in most of the motion phase. Indeed, tDA_k is only below this level at the beginning of the motion phase, from 0 to 0.50 s for condition 1 and from 0 to 0.65 s for condition 2 with EEG signals of the uninjured motor cortex [see Fig. 4(b)], and from 0 to 0.50 s for condition 1 and from 0 to 0.70 s for condition 2 with EEG signals of both the uninjured and injured motor cortex [see Fig. 4(c)]. Notice that the time required to achieve significant tDA_k in the motion phase was higher in condition 2 (i.e., in the attempt to move the affected arm) than in condition 1 (i.e., the movement of the unaffected arm). These results show significant continuous decoding of movement using EEG activity from the contralesional motor cortex.

A summary of the decoding accuracy metrics (DA_{rest}, DA_{motion}, and DA_{total}) for each participant and the average across all of them in the two experimental conditions is presented in Table II. With brain signals from the injured motor cortex [see Table II(a)], DA_{rest} is above the chance level for all participants (average of 91 ± 7 and 96 ± 4 for condition 1 and 2, respectively), however, DA_{motion} is always below this level (average of 38 ± 11 and 24 ± 7 for condition 1 and 2, respectively), thus none of the participants achieved significant continuous decoding of movement. With brain signals from the uninjured motor cortex and from both the injured and uninjured motor cortex [see Table II(b) and (c)], DA_{rest} in both experimental conditions is above the chance level for all participants (using the uninjured motor cortex, average of 84 ± 10 and 84 ± 8 for condition 1 and 2, respectively; using both the injured and uninjured motor cortex, average of 86 ± 9 and 86 ± 7 for condition 1 and 2, respectively), while DA_{motion} is above this level in all participants for condition 1 (using the uninjured motor cortex, average of 71 ± 13; using both the injured and uninjured motor cortex, average of 72 ± 13), and in four out of six participants for condition 2 (using the uninjured motor cortex, average of 62 ± 14; using both the injured and uninjured motor cortex, average of 69 ± 20; participants P2 and P5 did not achieve DA_{motion} above the chance level). These subject-specific results show significant continuous decoding of movement with EEG signals of the uninjured motor cortex. Thus, the subsequent analysis are based only on EEG activity from the contralesional motor cortex.

tDA_k was also computed for the decoding model based on the SVM alone, and the values of this metric were above chance level in most of the rest and motion phases (tDA_k was below chance level from -0.15 to 0.20 s in condition 1, and from -0.15 to 0.25 s in condition 2). However, they were both

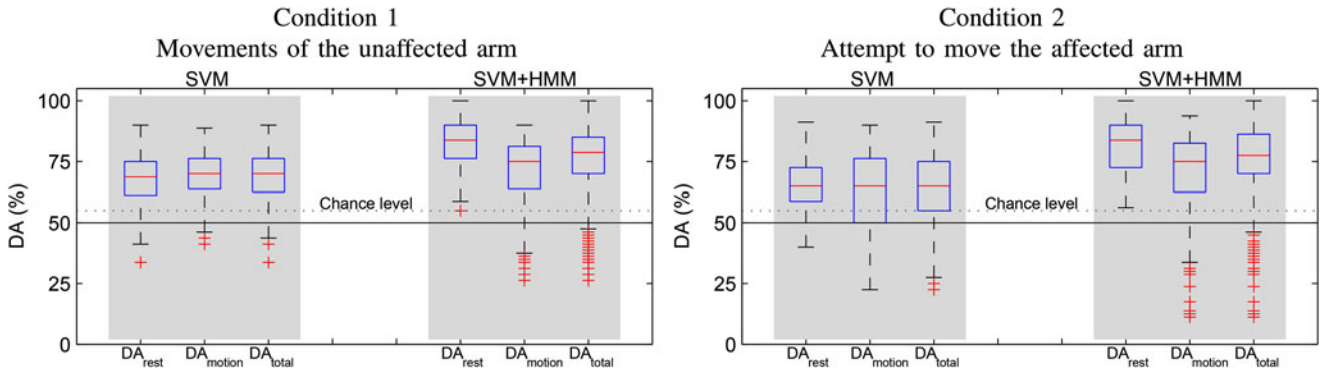

Fig. 5. Distributions of DA_{rest}, DA_{motion}, and DA_{total} across all participants for the decoding model based on SVM and for the one SVM+HMM using EEG signal from the uninjured motor cortex. The dotted line in all plots indicates the chance level.

lower than for the decoding model based on SVM+HMM. Fig. 5 shows the distributions of decoding accuracy metrics DA_{rest}, DA_{motion}, and DA_{total} across all participants for the proposed decoding model SVM+HMM and for the one based on SVM alone. For both decoding models and in the two conditions, the median of the distributions of DA_{rest}, DA_{motion}, and DA_{total} were significantly different ($p < 0.05$, Wilcoxon signed-rank test) and higher than the chance level. However, in the two conditions, the median of the difference between SVM+HMM and SVM for DA_{rest}, DA_{motion}, and DA_{total} was significantly different form zero ($p < 0.05$, paired Wilcoxon signed-rank test). In condition 1, the averaged values of DA_{rest}, DA_{motion}, and DA_{total} for the decoding model SVM+HMM ($84\% \pm 10$, $71\% \pm 13$ and $77\% \pm 11$, respectively) were higher than for the decoding model based on SVM alone ($68\% \pm 8$, $69\% \pm 7$ and $69\% \pm 10$, respectively). In condition 2, the averaged values of DA_{rest}, DA_{motion}, and DA_{total} for the decoding model SVM+HMM ($84\% \pm 8$, $62\% \pm 14$ and $72\% \pm 11$, respectively) were also higher than for the decoding model based on SVM alone ($66\% \pm 4$, $66\% \pm 7$ and $64\% \pm 14$, respectively).

The distributions of the decoding accuracy metrics DA_{rest}, DA_{motion}, and DA_{total} for the decoding model based on SVM+HMM were also examined for each participant individually. In condition 1, the median of the distributions of these metrics were significantly different ($p < 0.05$, Wilcoxon signed-rank test) and higher than the chance level for all the participants. In condition 2, the median of the distribution of DA_{rest} was significantly different ($p < 0.05$, Wilcoxon signed-rank test) and above chance level in all participants, while for DA_{motion} and DA_{total} they were significantly different ($p < 0.05$, Wilcoxon signed-rank test) and above chance level in four out of the six participants (participants P2 and P5 presented decoding accuracy metrics below the chance level).

In summary, these results show significant decoding accuracy in the continuous estimation of the unaffected (six out of six participants) and affected (four out of six participants) limb movement from EEG activity of the uninjured motor cortex in chronic stroke survivors.

IV. Discussion

This study shows the possibility of building a continuous decoder of movement of paralyzed limbs from the EEG activity of the contralesional uninjured motor cortex of severe chronic stroke patients. The event-related power desynchronization maps revealed significant cortical activation in the uninjured motor cortex in both motor conditions, with lower desynchronization during the attempt to move the affected limb than during movement of the unaffected limb. No significant cortical activation was observed in the injured cortex. The EEG signatures of event-related power desynchronization maps were different across patients with respect to the electrodes and frequency bands, which could be attributed to the different degrees of cortical lesion, the rehabilitative status of each participant (all participants were chronic but with different time elapsed since the seizure) or to simple individual differences.

The power decrease observed during the attempt to move the affected arm indicated that the uninjured cortex is involved in the attempt to move the ipsilateral side of the body, in line with previous studies [28], [30]. Interconnection circuits between both hemispheres could explain the existence of this ipsilateral activity [33]. Previous studies have revealed that the ipsilateral cerebral cortex plays a role in motor planning and execution [54], [55], and that subtle motor deficits appeared in the unaffected limbs after unilateral stroke [56], [57]. Other studies based on EEG signals have reported the existence (in the same hemisphere) of cortical rhythms associated with ipsilateral movements that can be distinguished from the cortical rhythms associated with contralateral movements [29], [34], [58]. This body of evidence, together with the results presented herein, suggests that EEG signals from the uninjured motor cortex of stroke survivors could be used to obtain movement information associated with the paralyzed side of the body.

Therefore, this study investigates if EEG signals from the contralesional motor cortex can be used to decode the attempt to move the paralyzed upper limb. Notice that a continuous estimation of the attempt to move could provide users of BCIs or robot-assisted rehabilitation systems (i.e., the patients) with a new natural, easy, and intuitive way to control external mobility

devices. This is very different from the classical approaches that are based on distinguish patterns in the brain signals associated with external events or the autoregulation of sensorimotor rhythms. The results showed that it is possible to build a continuous EEG-based decoder of movement for paralyzed chronic stroke patients. The time-resolved decoding accuracy (tDA_k) for both type of movements was significant and above chance level for the entire rest phase and during most of the motion phase (except for the short time interval at movement initiation). In particular, the low tDA_k initiates at the movement onset and lasted 0.50 and 0.65 s for movements of the unaffected and affected arms, respectively. These results are due to the high variability of the power spectral features at the change from rest to motion, and also because in the time interval $(0, \delta)$, the EEG signals used span over the rest and motion periods. Consequently, power spectral features at the beginning of the motion phase are less discriminative. In this respect, the continuous decoding was evaluated by assuming the power spectral features within $(0, \delta)$ s to belong to either the rest or motion phase; however, tDA_k was always below chance level just after the movement initiation up to a specific time (around one second in all cases), where it was again significant and above chance level.

The overall decoding accuracies (DA_{rest}, DA_{motion}, and DA_{total}) across all participants were significant and above chance level for both conditions. However, these accuracies were slightly lower in the attempt to move the affected arm ($84\% \pm 08$, $62\% \pm 14$, and $72\% \pm 11$, respectively) than during the movement of the unaffected arm ($84\% \pm 10$, $71\% \pm 13$, and $77\% \pm 11$, respectively). This might be because the power spectral features were computed from the EEG signals of the uninjured motor cortex, which were less discriminative when trying to move the affected ipsilateral arm. These results are encouraging, considering the fact that there was no mental task or specific mental strategy assigned to or learned by the participants during the experiment; rather, the participants executed—or attempted to do so—natural reaching movements. Moreover, data were collected from only one experimental session and the patients did not receive any type of feedback. Consequently, it could not promote any reorganization of the motor rhythms by learning.

The results achieved with the combination of HMM and SVM showed that the structure of interventions can be useful to improve decoding accuracy, since they resulted in significantly better decoding results than simple SVM. HMM models have been used before to distinguish different states during motor tasks [49]–[51], but they have not been exploited to detect attempt of movement. Instead, detection of motion is usually based on a sliding window (see [36], [48], [59] for stroke and [22], [60] for spinal cord injury). Although these methods use the whole motor cortex and include features based on motor related cortical potentials, we believe they could benefit from modeling the temporal structure to obtain better accuracies.

Although not reported in the paper, the decoder was also tested using as movement onset the cue that instructed the participants to perform or to attempt to perform the movement. This aimed to understand how the proposed decoding model expands to stroke patients without any residual EMG activity (i.e., when it is not possible to obtain the movement onset from the EMG). While the time resolved and the overall decoding accuracy results were similar to those obtained when using the movement onset the EMG activity, the main difference was a longer time (1.0 and 1.1 s, for movements of the unaffected arm and for the attempt to move the affected arm, respectively) to achieve significant decoding in the transition from rest to motion. This could be due to different delays to start movement in the execution of the experiments. Despite this, the proposed decoding model could be applied to rehabilitation scenarios with patients without residual EMG activity.

During rehabilitation therapies, it is common for stroke survivors to compensate the movement of paretic limbs by using the unaffected body side. This may artificially boost decoding performance by exploiting neural correlates originated by the compensatory movements. Since the current study aimed to show that there exists useful ipsilateral activity to decode motion, strict exclusion criteria were applied resulting in 6 discharged participants out of 12. In addition, for the accepted participants we carried out an extra check based on the average of EMG amplitude in the rest and motion phases for both arms and for both conditions (see Table S1 in the supplementary results). Results show that when the participants attempted to move the affected arm (condition 2), the EMG activity in the affected arm was several orders higher in the motion phase than in the rest phase, whereas in the unaffected arm it was of the same order in the rest and motion phases. Thus, no movement of the unaffected arm is present during the attempt to move the paretic limb. It is interesting to note that an alternative way to control false positives would be to decode what limb the patient is moving or attempting to move. It is a part of the future work to investigate the detection of the moved limb in stroke patients from EEG, however, this will require a different experimental protocol to the one followed in this paper.

The proposed decoding model is expected to be used in real BCI-based rehabilitation scenarios, but the work and results presented herein are based on offline analysis. Although all the decoding algorithms (i.e., causal filters, the autoregressive spectrum, the SVM and the HMM) can directly be used in an online system, it is necessary to further validate the results on real rehabilitation procedures. Decoding performances may vary due to compensatory movements, the closed loop nature of rehabilitation and the patient's personal evolution.

Note that the traditional way to achieve motor relearning in stroke survivors is to carry out rehabilitation therapies to enhance the lost activity in the damaged side, i.e., to focus in the lesional and perilesional areas [61], [62]. For instance, brain signals from the injured hemisphere have been used to induce ipsilesional BCI-based control in stroke survivors demonstrating BCI's efficacy in inducing motor functional rehabilitation [63]. However, this is not always satisfactory as the damaged hemisphere might be functionally altered [27]. Because of this, the usage of brain signals from the contralesional side has become an interesting alternative to decode motor information associated with paralyzed limbs. Therefore, BCIs rehabilitation scenarios based on decoding motor information of the paretic limbs using brain signals of the uninjured motor cortex could

be viewed as an interesting alternative to regain fast and natural motor control. Moreover, this might promote ipsilesional function recovery via subcortical or cortical interhemispheric connections, thus, providing a great potential to achieve motor relearning. Although this aspect still requires further investigation, the proposed approach has clinical relevance as it involves a novel and interesting alternative to extract motor information that is useful to obtain control signals for BCIs, assistive technologies, and rehabilitation robotics, whose application could promote brain reorganization.

Despite these theoretical considerations, most of the successful rehabilitation efforts in chronic stroke [14] rely on the fact that therapeutic reorganization of the ipsilesional cortex induced by functional activities of the paralyzed limbs predicts a more positive outcome. Nonetheless, patients with complete interruption of the cortical command to the periphery (i.e., without any remaining EMG activity during movement attempts and no motor evoked potentials after ipsilesional transcranial magnetic stimulation) may benefit at least for proximal arm control from ipsilateral BCIs [64]. Long-term ipsilateral motor control may however impede or block ipsilesional reorganization through an overuse of the healthy hemisphere and learned nonuse of the ipsilesional sites [10], [65], [66]. This may—over an unknown time period—compensate for the improvements achieved with ipsilateral movement control. It remains an open question how the brain handles these contradictory forces over time. The present rudimentary knowledge behind brain reorganization after stroke induced by the different strategies to regain motor control do not allow any firm predictions. On the other hand, forced reuse of the paralyzed limb through an ipsilateral BCI may strengthen the ipsilateral efferent outflow neuronal networks due to the proprioceptive and visual feedback plus reward from successful hand movements. This may lead to therapeutic improvement if the ipsilateral BCI is applied on a continuous basis in real life contexts.

V. Conclusion

This study investigated the continuous decoding of the attempt to move paralyzed limbs from electroencephalographic brain signals recorded from the contralesional uninjured motor cortex of chronic stroke survivors. The analysis of the EEG activity revealed the presence of significant oscillatory activity in the uninjured hemisphere associated with the attempt to move the upper limb in the paretic side of the body. This oscillatory activity and a decoding model that exploits the temporal structure of the intervention were employed to continuously detect the attempt to move the paralyzed limb and significant decoding accuracy results were obtained. The proposed framework of continuous decoding using EEG brain signals from the uninjured cortex could provide to stroke patients with a natural, easy, and intuitive way to achieve control of BCIs or robot-assisted rehabilitation devices.

References

[1] N. Sharma and L. G. Cohen, "Recovery of motor function after stroke," *Develop. Psychobiol.*, vol. 54, no. 3, pp. 254–262, 2010.

[2] H. S. Jorgensen *et al.*, "Outcome and time course of recovery in stroke. The Copenhagen stroke study," *Archives Phys. Med. Rehabil.*, vol. 76, pp. 399–412, 1995.

[3] P. Langhorne *et al.*, "Motor recovery after stroke: A systematic review," *Lancet Neurol.*, vol. 8, no. 8, pp. 741–754, 2009.

[4] R. Riener *et al.*, "Patient-cooperative strategies for robot-aided treadmill training: First experimental results," *IEEE Trans. Neural Syst. Rehabil. Eng*, vol. 13, no. 3, pp. 380–394, Sep. 2005.

[5] P. Langhorne *et al.*, "Stroke rehabilitation," *Lancet*, vol. 377, pp. 1693–1702, 2011.

[6] C. D. Takahashi *et al.*, "Robot-based hand motor therapy after stroke," *Brain*, vol. 131, no. 2, pp. 425–437, 2008.

[7] H. I. Krebs *et al.*, "A working model of stroke recovery from rehabilitation robotic practitioners," *J. Neuroeng. Rehabil.*, vol. 25, no. 6, pp. 1–8, 2009.

[8] O. Fukuda *et al.*, "EMG based human-robot interface for rehabilitation aid," in *Proc. IEEE Int. Conf. Robot. Autom.*, 1998, no. 4, pp. 3492–3497.

[9] L. Dipietro *et al.*, "Customized interactive robotic treatment for stroke: EMG-triggered therapy," *IEEE Trans. Neural Syst. Rehabil. Eng.*, vol. 13, no. 3, pp. 325–334, Sep. 2005.

[10] J. W. Krakauer, "Motor learning: Its relevance to stroke recovery and neurorehabilitation," *Curr. Opin. Neurol.*, vol. 19, no. 1, pp. 84–90, 2006.

[11] X. L. Hu *et al.*, "A comparison between electromyography-driven robot and passive motion device on wrist rehabilitation for chronic stroke," *Neurorehabil. Neural Repair*, vol. 23, no. 8, pp. 837–846, 2009.

[12] E. Buch *et al.*, "Think to move: A neuromagnetic brain-computer interface (BCI) system for chronic stroke," *Stroke*, vol. 39, no. 3, pp. 910–917, 2008.

[13] K. K. Ang *et al.*, "Clinical study of neurorehabilitation in stroke using EEG-based motor imagery brain-computer interface with robotic feedback," in *Proc. 32nd Annu. Int. IEEE EMBS Conf.*, 2010, pp. 5549–5552.

[14] J. J. Daly and J. R. Wolpaw, "Brain-computer interfaces in neurological rehabilitation," *Lancet Neurol*, vol. 7, pp. 1032–1043, 2008.

[15] A. Caria *et al.*, "Chronic stroke recovery after combined BCI training and physiotherapy: A case report," *Psychophysiology*, vol. 48, no. 4, pp. 578–582, 2011.

[16] L. Crow and B. C. H. van der Wel, "Hierarchical properties of the motor function sections of the Fugl-Meyer assessment scale for people after stroke: A retrospective study," *Phys. Ther.*, vol. 88, no. 12, pp. 1554–1557, 2009.

[17] G. Pfurtscheller and F. H. L. da Silva, "Event-related EEG/MEG synchronization and desynchronization: Basic principles," *Clin. Neurophysiol.*, vol. 110, no. 11, pp. 1842–1857, Nov. 1999.

[18] D. J. McFarland *et al.*, "Mu and beta rhythm topographies during motor imagery and actual movements." *Brain Topogr.*, vol. 12, no. 3, pp. 177–186, 2000.

[19] H. Lakany and B. Conway, "Understanding intention of movement from electroencephalograms," *Expert Syst.*, vol. 24, no. 5, pp. 295–304, 2007.

[20] I. K. Niazi *et al.*, "Detection of movement intention from single-trial movement-related cortical potentials," *J. Neural Eng.*, vol. 8, no. 6, 2011, Art. no. 066009.

[21] L. Kauhanen *et al.*, "EEG-based brain-computer interface for tetraplegics," *Comput. Intell. Neurosci.*, vol. 2007, pp. 1–11, 2007.

[22] E. pez-LóLarraz *et al.*, "Continuous decoding of motor attempt and motor imagery from EEG activity in spinal cord injury patients," in *Proc. 34th Annu. Int. IEEE EMBS Conf.*, 2012, pp. 1798–1801.

[23] O. Bai *et al.*, "Towards a user-friendly brain-computer interface: Initial tests in ALS and PLS patients," *Clin. Neurophysiol.*, vol. 121, no. 8, pp. 1293–1303, 2010.

[24] T. Ono *et al.*, "Brain-computer interface with somatosensory feedback improves functional recovery from severe hemiplegia due to chronic stroke," *Front. Neuroeng.*, vol. 7, 2014, Art. no. 19.

[25] K. K. Ang *et al.*, "Brain-computer interface-based robotic end effector system for wrist and hand rehabilitation: Results of a three-armed randomized controlled trial for chronic stroke," *Front. Neuroeng.*, vol. 7, 2014, Art. no. 30.

[26] E. Chung *et al.*, "Effects of brain-computer interface-based functional electrical stimulation on brain activation in stroke patients: A pilot randomized controlled trial," *J. Phys. Ther. Sci.*, vol. 27, no. 3, pp. 559–562, 2015.

[27] R. J. Seitz *et al.*, "Neuroimaging advances in stroke rehabilitation," *US Neurology*, vol. 6, no. 2, pp. 105–111, 2010.

[28] L. Leocani and G. Comi, "Movement-related event-related desynchronization in neuropsychiatric disorders," *Prog. Brain Res.*, vol. 159, pp. 351–366, 2006.

[29] K. J. Wisneski *et al.*, "Unique cortical physiology associated with ipsilateral hand movements and neuroprosthetic implications," *Stroke*, vol. 39, no. 12, pp. 3351–3359, 2008.
[30] M. Stepien *et al.*, "Event-related desynchronization of sensorimotor EEG rhythms in hemiparetic patients with acute stroke," *Neurosci. Lett.*, vol. 488, no. 1, pp. 17–21, 2011.
[31] G. Hotson *et al.*, "Coarse electrocorticographic decoding of ipsilateral reach in patients with brain lesions," *PLoS One*, vol. 9, no. 12, Dec. 2014, Art. no. e115236.
[32] H. Johansen-Berg *et al.*, "The role of ipsilateral premotor cortex in hand movement after stroke," *Proc. Nat. Acad. Sci. USA*, vol. 99, no. 22, pp. 14518–14523, 2002.
[33] M. Kobayashi *et al.*, "Ipsilateral motor cortex activation on functional magnetic resonance imaging during unilateral hand movements is related to interhemispheric interactions," *NeuroImage*, vol. 20, pp. 2259–2270, 2003.
[34] D. T. Bundy *et al.*, "Using ipsilateral motor signals in the unaffected cerebral hemisphere as a signal platform for brain-computer interfaces in hemiplegic stroke survivors," *J. Neural Eng.*, vol. 9, no. 3, 2012, Art. no. 036011.
[35] J. M. Antelis *et al.*, "Continuous decoding of intention to move from contralesional hemisphere brain oscillations in severely affected chronic stroke patients," in *Proc. 34th Annu. Int. IEEE EMBS Conf.*, 2012, pp. 4099–4103.
[36] J. Ibánez *et al.*, "Detection of the onset of upper-limb movements based on the combined analysis of changes in the sensorimotor rhythms and slow cortical potentials," *J. Neural Eng.*, vol. 11, no. 5, 2014, Art. no. 056009.
[37] B. Hjorth, "An on-line transformation of EEG scalp potentials into orthogonal source derivations," *Electroencephalogr. Clin. Neurophysiol.*, vol. 39, pp. 526–530, 1974.
[38] C. Tallon-Baudry *et al.*, "Oscillatory gamma-band (30-70 Hz) activity induced by a visual search task in humans," *J. Neurosci.*, vol. 17, no. 2, pp. 722–734, Jan. 1997.
[39] H. Yuan *et al.*, "Relationship between speed and EEG activity during imagined and executed hand movements," *J. Neural Eng.*, vol. 7, no. 2, 2010, Art. no. 26001.
[40] B. Graimann and G. Pfurtscheller, "Quantification and visualization of event-related changes in oscillatory brain activity in the time frequency domain," *Prog. Brain Res.*, no. 159, pp. 79–97, 2006.
[41] J. Gross *et al.*, "Dynamic imaging of coherent sources: Studying neural interactions in the human brain," *Proc. Nat. Acad. Sci. USA*, vol. 98, no. 2, pp. 694–699, 2001.
[42] A. C. Evans *et al.*, "3D statistical neuroanatomical models from 305 MRI volumes," in *Proc. IEEE Nucl. Sci. Symp. Conf. Rec.*, 1999, vol. 3, pp. 1813–1817.
[43] D. J. McFarland and J. R. Wolpaw, "Sensorimotor rhythm-based brain-computer interface (BCI): Model order selection for autoregressive spectral analysis," *J. Neural Eng.*, vol. 5, no. 2, pp. 155–162, 2008.
[44] D. J. McFarland *et al.*, "Electroencephalographic (EEG) control of three-dimensional movement," *J. Neural Eng.*, vol. 7, 2010, Art. no. 036007.
[45] R. Bos *et al.*, "Autoregressive spectral estimation by application of the Burg algorithm to irregularly sampled data," *IEEE Instrum. Meas. Mag.*, vol. 51, no. 6, pp. 1289–1294, Dec. 2002.
[46] R. G. Steel and J. H. Torrie, *Principles and Procedures of Statistics With Special Reference to the Biological Sciences*. New York, NY, USA: McGraw-Hill, 1960.
[47] F. Lotte *et al.*, "A review of classification algorithms for EEG-based brain-computer interfaces." *J. Neural Eng.*, vol. 4, no. 2, pp. R1–R13, 2007.
[48] A. I. Sburlea *et al.*, "Continuous detection of the self-initiated walking pre-movement state from EEG correlates without session-to-session recalibration," *J. Neural Eng.*, vol. 12, no. 3, 2015, Art. no. 036007.
[49] B. Obermaierb *et al.*, "Hidden Markov models for online classification of single trial EEG data," *Pattern Recognit. Lett.*, vol. 22, no. 12, pp. 1299–1309, 2001.
[50] S. Chiappa and S. Bengio, "HMM and IOHMM modeling of EEG rhythms for asynchronous BCI systems," in *Proc. Eur. Symp. Artif. Neural Netw.*, 2004, pp. 193–204.
[51] H.-I. Suk and S.-W. Lee, "Two-layer hidden Markov models for multi-class motor imagery classification," in *Proc. 1st Workshop Brain Decoding: Pattern Recog. Challenges Neuroimaging*, 2010, pp. 5–8.
[52] T. fan Wu *et al.*, "Probability estimates for multi-class classification by pairwise coupling," *J. Mach. Learn. Res.*, vol. 5, pp. 975–1005, 2003.
[53] D. Garrett *et al.*, "Comparison of linear, nonlinear, and feature selection methods for EEG signal classification," *IEEE Trans. Neural Syst. Rehabil. Eng.*, vol. 11, no. 2, pp. 141–144, Jun. 2003.
[54] T. Verstynen *et al.*, "Ipsilateral motor cortex activity during unimanual hand movements relates to task complexity," *J. Neurophysiol.*, vol. 93, no. 3, pp. 1209–1222, 2005.
[55] S. Y. Schaefer *et al.*, "Ipsilesional motor deficits following stroke reflect hemispheric specializations for movement control," *Brain*, vol. 130, no. 8, pp. 2146–2158, 2007.
[56] O. Noskin *et al.*, "Ipsilateral motor dysfunction from unilateral stroke: Implications for the functional neuroanatomy of hemiparesis," *J. Neurol. Neurosurg. Psychiatry.*, vol. 79, pp. 401–406, 2008.
[57] S. Y. Schaefera *et al.*, "Hemispheric specialization and functional impact of ipsilesional deficits in movement coordination and accuracy," *Neuropsychologia*, vol. 47, no. 13, pp. 2953–2966, 2009.
[58] C. Gerloff *et al.*, "Multimodal imaging of brain reorganization in motor areas of the contralesional hemisphere of well recovered patients after capsular stroke," *Brain*, vol. 129, no. 3, pp. 791–808, Mar. 2006.
[59] J. Ibánez *et al.*, "Detection of the onset of voluntary movements based on the combination of ERD and BP cortical patterns," in *Proc. 2nd Int. Conf. NeuroRehabil.*, 2014, vol. 7, pp. 437–446.
[60] E. López-Larraz *et al.*, "Continuous decoding of movement intention of upper limb self-initiated analytic movements from pre-movement EEG correlates," *J. Neuroeng. Rehabil.*, vol. 11, no. 1, 2014, Art. no. 153.
[61] F. Tecchioa *et al.*, "Brain plasticity in recovery from stroke: An MEG assessment," *Neuroimage*, vol. 32, no. 3, pp. 1326–1334, 2006.
[62] Y. Dong *et al.*, "Evolution of FMRI activation in the perilesional primary motor cortex and cerebellum with rehabilitation training-related motor gains after stroke: A pilot study." *Neurorehabil. Neural Repair*, vol. 21, no. 5, pp. 412–428, 2007.
[63] A. Ramos-Murguialday *et al.*, "Brain-machine interface in chronic stroke rehabilitation: A controlled study," *Ann. Neurol.*, vol. 74, no. 1, pp. 100–108, 2013.
[64] K. Ganguly *et al.*, "Cortical representation of ipsilateral arm movements in monkey and man," *J. Neurosci.*, vol. 29, pp. 12948–12956, 2009.
[65] E. Taub *et al.*, "Constraint-induced movement therapy: A new family of techniques with broad application to physical rehabilitation—A clinical review," *J. Rehabil. Res. Develop.*, vol. 36, no. 3, pp. 237–251, 1999.
[66] V. Pomeroy *et al.*, "Neurological principles and rehabilitation of action disorders: Rehabilitation interventions," *Neurorehabil. Neural Repair*, vol. 25, no. 5, pp. 33S–43S, 2011.

Authors' photographs and biographies not available at the time of publication.